

Original paper

# Vegrandisite ( $\text{BaCl}_2$ ) a new mineral from salt melt inclusions from the Biely Vrch porphyry gold deposit, Slovakia

Peter KODĚRA<sup>1\*</sup>, Juraj MAJZLAN<sup>2</sup>, Kilian POLLOK<sup>2</sup>, František ŠIMKO<sup>3</sup>

<sup>1</sup> Department of Mineralogy, Petrology and Economic Geology, Faculty of Natural Sciences, Comenius University, Ilkovičova 6, 842 15 Bratislava, Slovakia; peter.kodera@uniba.sk

<sup>2</sup> Institute of Geosciences, Friedrich Schiller University Jena, Burgweg 11, D-07749 Jena, Germany

<sup>3</sup> Institute of Inorganic Chemistry, Slovak Academy of Sciences, Dúbravská cesta 9, 845 36 Bratislava, Slovakia

\* Corresponding author



The new mineral vegrandisite ( $\text{BaCl}_2$ ) was discovered at the porphyry gold deposit Biely Vrch, 3.5 km southeast of the town Detva, in the Central Slovak Volcanic Field. It occurs as a minor phase in salt melt inclusions hosted by vein quartz, where it forms small anhedral and transparent crystals up to 4  $\mu\text{m}$  long, accompanied by halite and several other daughter minerals, mainly javorieite, rinneite, chlorocalcite and hibbingite. Vegrandisite was identified by techniques embedded in transmission electron microscopy but many mineral properties, including optical and structural ones, are known from the synthetic  $\text{BaCl}_2$  analogue. Strongest bands in the Raman spectra include 114, 125, 187  $\text{cm}^{-1}$  and in the IR spectra in the region between 2852 and 2944  $\text{cm}^{-1}$ . Vegrandisite in inclusions approaches the composition of  $\text{BaCl}_2$ , but Sr (up to ~4.5 wt. %) and Br (up to ~2.1 wt. %) are also incorporated. It is orthorhombic, belongs to the space group *Pnma*. Obtained unit-cell parameters  $a = 7.80(3)$  Å;  $b = 4.71(2)$  Å;  $c = 9.60(9)$  Å,  $V = 352.68(54)$  Å<sup>3</sup> are consistent with the published parameters of  $\alpha$ - $\text{BaCl}_2$  that exhibits a  $\text{PbCl}_2$ -type (cotunnite) structure. Solid phases in salt melt inclusions, including vegrandisite, have crystallized from the salt melt on cooling of the inclusions. Late crystallization of  $\text{BaCl}_2$  is related to accumulation of the incompatible element barium in the residual salt melt. Parental salt melt evolved from a hypersaline liquid, accompanied by a magmatic vapor, that were exsolved from a shallow dioritic magma.

**Keywords:** barium chloride, salt melts, fluid inclusion, FIB, daughter mineral

**Received:** 23 July 2025; **accepted:** 26 November 2025; **handling editor:** J. Zachariáš

## 1. Introduction

Salt melt inclusions represent a rare type of fluid inclusions which trapped a hypersaline liquid at high temperature. At room temperature, the entire volume of the inclusions is occupied by several salt crystals and a distorted vapor bubble, but a liquid phase is absent. The more common high-salinity aqueous inclusions still contain a liquid aqueous solution at room temperature. Salt melt inclusions are found in shallow magmatic-hydrothermal systems, typically associated with Cu–Au porphyry, skarns and magnetite-apatite mineralisations (e.g., Campos et al. 2002; Fulignati et al. 2001; Rottier et al. 2016; Kozák et al. 2017; Xu et al. 2023; Simón et al. 2024; Xu et al. 2024), including several porphyry gold systems in the Central Slovak Volcanic Field in the Western Carpathians (Koděra et al. 2014).

The absence of aqueous liquid in salt melt inclusions at room temperature enables crystallisation of various anhydrous chloride and fluoride minerals that do not occur in hypersaline inclusions, because many of these minerals are hygroscopic and thus, they are not stable in contact with aqueous solutions. Thus, a combination

of several indirect, unconventional methods needs to be applied, accompanied by comparison with data from synthetic phases, to provide a reliable information about the chemistry and crystallography of these minerals. During the last decade, a significant progress was made in the identification of the most common solid phases that occur in salt melt inclusions, including the new mineral javorieite (Koděra et al. 2017), as well as chlorocalcite (Grishina et al. 2018), rinneite (Grishina et al. 2020) and hibbingite (Koděra et al. 2022).

In this work, we describe a new mineral that precipitated in inclusions from salt, chloride-rich melts in a porphyry deposit Biely Vrch in Slovakia. Vegrandisite, with nominal composition  $\text{BaCl}_2$ , occurs in an assemblage with a number of other chlorides in inclusions hosted by quartz. The new mineral (IMA2023-045), its name and symbol (Veg) have been approved by the Commission on New Minerals, Nomenclature and Classification (CNMNC) of the International Mineralogical Association (IMA) (Bosi et al. 2024).

In inorganic chemistry, there are known four polymorphic modifications of  $\text{BaCl}_2$  and all of them are structurally well characterized. Under ambient conditions,  $\alpha$ -form

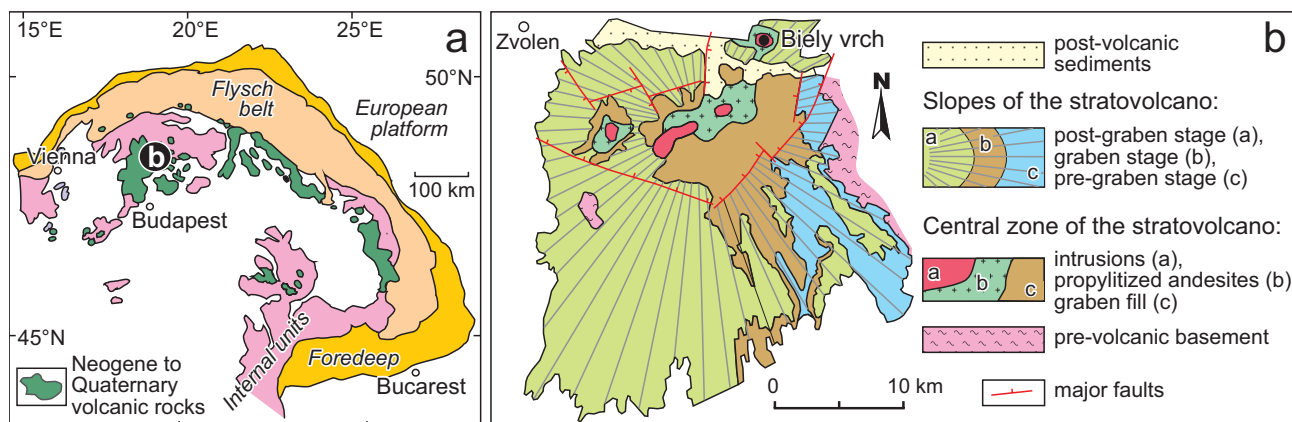


**Fig. 1a** – Regional geological setting of the Central Slovak Volcanic Field (CSVF) among the Neogene to Quaternary volcanic rocks of the Carpathian arc and the Pannonian basin (after Lexa et al. 1999). Black circle shows the position of the Javorie stratovolcano. **b** – Structural scheme of the Javorie stratovolcano, including location of the Biely Vrch porphyry gold deposit (after Koděra et al. 2018).

of  $BaCl_2$  crystallizes in the orthorhombic  $Pnma$  structure (Brackett et al. 1963). Above  $925^\circ C$ , cubic  $\beta$ - $BaCl_2$  occurs with the  $Fm\bar{3}m$  structure. According to Haase and Brauer (1978) and Liu and Eick (1989), there also exists a metastable hexagonal phase of  $BaCl_2$  with the anti- $Fe_2P$  structure ( $P62m$ ) and a monoclinic structure crystallises at high pressures of 7–10 GPa. As presented below, vegrandisite corresponds to the orthorhombic modification of  $BaCl_2$ .

## 2. Geological settings, occurrence, and mineral association

Vegrandisite was identified as a minor daughter mineral in salt melt inclusions hosted in vein quartz in the porphyry Au deposit Biely Vrch ( $48^\circ 33' 31'' N$ ,  $19^\circ 22' 28'' E$ ) in the Javorie stratovolcano, which is a part of the Central Slovak Volcanic Field (Fig. 1). This field of Middle Miocene Age is situated on the inner side of the Carpathian arc. Geographically, this deposit occurs 3.5 km southeast of the town Detva in central Slovakia. The porphyry deposit was discovered in 2006 by EMED Mining Ltd. (Hanes et al. 2010), and it represents an economic accumulation of gold ore (42 Mt at 0.8 g/t Au, www.emed-mining.com).

The salt melt inclusions hosted in quartz contain several other associated Cl-bearing minerals. Based

on interpretation of data on these inclusions obtained by combined Raman spectroscopy and transmission electron microscopy (TEM), the major phases in inclusions include halite (NaCl), javorieite ( $KFeCl_3$ ), chlorocalcite ( $KCaCl_3$ ), rinneite ( $KNa_3FeCl_6$ ) and hibbingite ( $Fe_2(OH)_3Cl$ ). Fluorite, scheelite/powellite and Ba-, Zn-, Pb-bearing chlorides (possibly flinteite ( $K_2ZnCl_4$ ) and an unknown Ba–Pb–Cl phase) represent minor phases in inclusions (Fig. 2) (Koděra et al. 2015, 2017, 2022). The techniques embedded in TEM used in these studies and this work are chemical analyses with energy-dispersive (EDX) spectrometry, structural analysis with selected-area electron diffraction (SAED) or electron back-scattered diffraction (EBSD). Samples were extracted in the form of thin lamellae with the site-specific focused ion beam (FIB) technique. *In situ* Raman spectroscopy also determined very rare presence of some salt hydrates ( $FeCl_2 \cdot 2H_2O$ ), magnetite, K-feldspar, pyroxene, scheelite and chalcopyrite.

## 3. Methodology

The new mineral vegrandisite was studied on a sample of a porous quartz vein from an inclined drill hole DVE-51 at a depth of 475.0 m along the hole at the porphyry Au deposit Biely Vrch. Porous texture of the vein is probably related to former presence

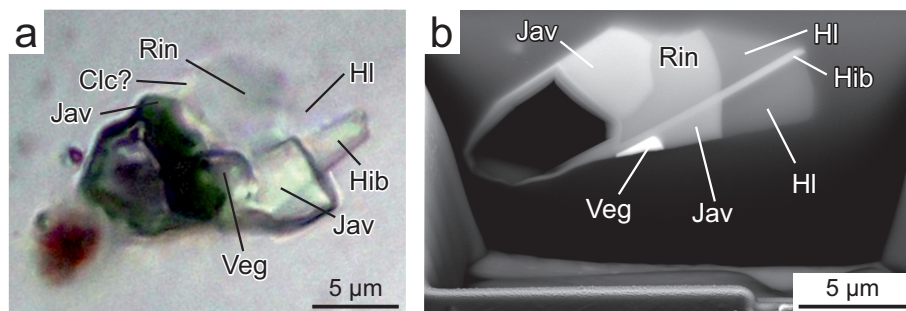


**Fig. 2** – Optical (a) and electron-optical images (b) showing the studied mineral assemblage with vegrandisite in salt melt inclusion in a quartz vein from the Biely Vrch deposit (sample DVE-51\_475.0). Identification of phases is based on combination of Raman spectroscopy and FIB-TEM-EDX-SAED analyses. Abbreviations: Clc = chlorocalcite, Veg = vegrandisite, Hib = hibbingite, HI = halite, Jav = javorieite, Rin = rinneite.

of salt melts that were dissolved by later aqueous fluids. For analyses a doubly polished wafer  $\sim 200\ \mu\text{m}$  thick was used.

Focused ion beam (FIB) extraction of the fluid-inclusion solid content was conducted using a FEI Quanta 3D FEG instrument. FIB enabled a progressive abrasion of a typical salt melt inclusion, using a focused beam of Ga ions, monitored by secondary electron (SE) and back-scattered electron (BSE) imaging. The gallium ion gun was operated at 30 kV with a beam current between 30–0.1 nA for sample preparation. A deposited platinum stripe was used to protect the surface. To remove amorphous layers on the FIB cut (which form during the preparation), the FIB sections were finally cleaned at 5 kV and 48 pA beam current. The extracted lamella was transferred into a transmission electron microscopy (TEM) and minerals in the inclusion were investigated to determine their chemical and structural properties as specified below.

Chemical composition of the minerals was measured with the TEM energy-dispersive (EDX) spectrometry, using a X-Maxn 80T SDD (Oxford Instruments) EDX detector in STEM mode by an area measurement with activated drift compensation.

To confirm that the studied Ba-Cl phase from the Biely Vrch salt melt inclusions is structurally identical to the  $\alpha$ -form of  $\text{BaCl}_2$ , we have used selected area electron diffraction (SAED) in a TEM on the FIB lamella. This combination ensures that the sample has a minimum contact to air as preparation and analysis are performed in high vacuum with a short transfer time ( $< 5$  minutes) between the instruments. TEM imaging and diffraction on the extracted lamella was performed with a FEI Tecnai G<sup>2</sup> FEG TEM, operating at 200 keV using a double tilt holder; all images were recorded by a 2K CCD camera (Gatan UltraScan). Two different zone axes were documented which allow to refine the lattice constants for a known crystal structure. Note that in the course of the TEM work on the salt melt inclusion, it was initially not anticipated to describe a new phase. The hygroscopic behaviour of the salt minerals in the inclusion did not allow the sample to measure again after removing it from the high vacuum of the TEM. The refinement of lattice constants using  $d$  values obtained from electron diffraction patterns on the same grain was performed using the UnitCell program (Holland and Redfern 1997).

Optical properties were determined on synthetic  $\text{BaCl}_2$  prepared by cooling of  $\text{BaCl}_2$  melt (Wulff and Heigl 1931; Winchel and Winchel 1989). This procedure led only to anhedral pieces of  $\text{BaCl}_2$ , thus limiting the available information. In the natural material, the determination of the optical properties was precluded by the small size of the mineral and by intimate intergrowths with other associated minerals.

Micro-Raman analysis of synthetic  $\text{BaCl}_2$  was performed using a DXR Raman microscope (Thermo Fisher Scientific, U.S.A). Raman spectra were obtained by rotating the powder sample, immersed in a sealed glass capillary. Spectra were excited at room temperature using the 532 nm line of a Nd:YAG laser, with power emission conditions of 5 mW on the sample surface. Objective lens of 100 $\times$  with a pinhole aperture of 50  $\mu\text{m}$  was used. Each spectrum was collected with exposure time of 5 s and 60 accumulations, to minimize accidental contamination by cosmic radiation. Peak position was calibrated using a 520  $\text{cm}^{-1}$  band of Si-wafer and using a neon lamp.

Micro-Raman analyses of daughter minerals in salt melt inclusions hosted in vein quartz were performed by a Horiba Jobin-Yvon LabRam HR800 spectrometer, equipped with an Olympus BX41 optical microscope in the laboratory of Earth Science Institute of the Slovak Academy of Sciences in Banská Bystrica, Slovakia. Polarized laser emission at  $\lambda = 532\ \text{nm}$  (frequency-doubled Nd:YAG laser) was used for excitation. The Raman-scattered light was collected in 180 $^\circ$  geometry through a 100 $\times$  objective lens with a numerical aperture of 0.8 and dispersed by a diffraction grating with a density 600 grooves/mm onto a Peltier cooled CCD detector Synapse (Horiba Jobin-Yvon). Spectra were collected in two acquisitions of 30 seconds in the range 70–4000  $\text{cm}^{-1}$ . The bands from a teflon standard were used to calibrate the spectrometer.

Due to the nature of the mineral, most physical and optical properties could not be established on the type material. However, because barium chloride is a well-known compound in inorganic chemistry, several of the properties could have been taken over from chemical literature.

The holotype material (quartz vein hosting the studied salt melt inclusions) was deposited in the Mineralogical Museum of the Comenius University at the Faculty of Natural Sciences in Bratislava, Ilkovičova 6, Bratislava 842 15, Slovakia, catalogue no. 7400. This sample is already deposited there (DVE-51/475.0), as the sample is also the holotype for another new mineral javorieite ( $\text{KFeCl}_3$ ), which is also hosted by salt melt inclusions in the same sample of vein quartz (Koděra et al. 2017).

## 4. Results and literature data on properties of the new mineral

### 4.1. Physical properties

Vegrandisite forms small anhedral transparent crystals, often attached to javorieite (Fig. 2), delimited by the surrounding crystals that precipitated from the salt melt before vegrandisite did. The size of individual grains

**Tab. 1** Normalized standardless semi-quantitative TEM-EDX point analyses of vegrandisite from the sample DVE-51\_475.0 after opening by FIB (in wt. %). Note that in the analyses the Fe and O signal from neighbouring phases and copper signal from grid have been ignored and the remaining signals were normalised to 100%. Chlorine from neighbouring chlorides (e.g., hibbingite) probably contribute to the signal in analysis 2.

anal.#	1	2
Ba	60.0	56.5
Sr	4.5	2.9
Cl	33.4	38.9
Br	2.1	1.7
Total	100.0	100.0
<i>apfu</i>		
Ba	0.90	0.79
Sr	0.11	0.06
Cl	1.94	2.11
Br	0.05	0.04
Total	3.00	3.00

depends on the size of inclusions – in 15  $\mu\text{m}$  long inclusions, vegrandisite reaches 4  $\mu\text{m}$ . The mineral is very hygroscopic and transform rapidly at room temperature to  $\text{BaCl}_2 \cdot 2\text{H}_2\text{O}$ , but loses one-half of its crystal  $\text{H}_2\text{O}$  if heated above 55  $^\circ\text{C}$ . By further heating, it returns to anhydrous  $\text{BaCl}_2$  at 121  $^\circ\text{C}$  (Ropp 2013).

Vegrandisite appears colourless in the natural samples. Synthetic material is white, with white streak and vitreous lustre. Based on X-ray excited luminescence of a  $\text{BaCl}_2$  crystal, there are three overlapping emission bands with peak wavelengths of 330, 410, and 530 nm. The maximum emission peak wavelength is approximately 390 nm (Kim et al. 2011). In UV light (254/365 nm),  $\text{BaCl}_2$  powder shows weak yellow luminescence.  $\text{BaCl}_2$  is brittle, the measured density is 3.856  $\text{g}\cdot\text{cm}^{-3}$  at 20  $^\circ\text{C}$  (Richards 1894; Winchel and Winchel 1989) and compares well to the calculated density of 3.92  $\text{g}\cdot\text{cm}^{-3}$  (based on lattice parameters

determined in this work and the content of the  $\text{BaCl}_2$  unit cell,  $Z = 4$ ). Magnetic susceptibility of  $-72.6 \times 10^{-6} \text{ cm}^3/\text{mol}$  was reported by Lidle (2010). Hardness, cleavage, or parting was not determined because of the hygroscopic nature of the synthetic material.

#### 4.2. Chemical properties

Due to the nature of the mineral, which is extremely liable to hydration and is exclusively present in tiny inclusions hosted by quartz, it was very difficult to obtain chemical analyses of this mineral. However, the FIB-TEM-EDX analytical technique enabled non-standardized semi-quantitative EDS analyses of the mineral, subsequently exposed to surface in vacuum. The tabulated best analysis of vegrandisite (Tab. 1) presents composition obtained at the same spot where electron diffraction data obtained by TEM-SAED were in general agreement with the structure of synthetic  $\alpha\text{-BaCl}_2$ . As the result of stray radiation from neighbouring phases, all analyses of vegrandisite also contain small signals from the host quartz and neighbouring solid phases (Fe, Si, O, Cl) as well as copper from the grid material and gallium from the FIB preparation (Fig. 3). Therefore, the formula of vegrandisite can only be determined semi-quantitatively and it is affected by a significant analytical error. The contributions from Fe and O have been ignored in the calculation of the formula. Despite of that, the chemical data clearly approach the stoichiometry and composition of  $\text{BaCl}_2$ , and they show that Sr (up to  $\sim 4.5$  wt. %) and Br (up to  $\sim 2.1$  wt. %) are also incorporated in this phase. Concentrations of  $\text{H}_2\text{O}$  and  $\text{CO}_2$  could not be determined directly due to the nature of the mineral, but we consider them not to be present, because the grain has a reasonable stability under the electron beam in TEM without

dehydration or degassing effects during electron imaging and EDX analyses. The empirical formula calculated on the basis of 3 atoms per formula unit in total is  $(\text{Ba}_{0.90}\text{Sr}_{0.11})_{\Sigma 1.01}(\text{Cl}_{1.94}\text{Br}_{0.05})_{\Sigma 1.99}$ , assuming that Sr substitutes for Ba, and Br substitutes for Cl. The simplified formula is  $(\text{Ba,Sr})(\text{Cl,Br})_2$  and the ideal formula is  $\text{BaCl}_2$

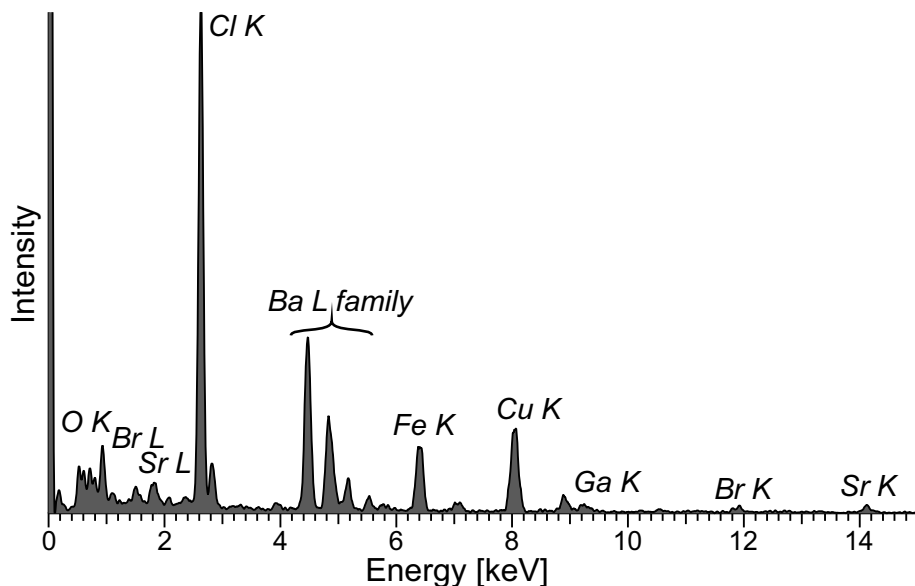


**Fig. 3** – EDS spectrum obtained from vegrandisite in the inclusion in the sample DVE-51\_475.0. The copper signal comes from grid and gallium results from the FIB preparation, while iron as well as oxygen come from phases close to vegrandisite in the inclusion.

which requires 65.95 wt. % barium and 34.05 wt. % chlorine.

Synthetic BaCl<sub>2</sub> is soluble in water, insoluble in acetone, ethanol and ether, slightly soluble in acetic acid and sulfuric acid (Ropp 2013).

#### 4.3. Crystallography and structural properties

TEM work on the studied salt melt inclusion enabled to obtain the following orthorhombic unit-cell parameters of vegrandisite:  $a = 7.80(3)$  Å;  $b = 4.71(2)$  Å;  $c = 9.60(9)$  Å,  $V = 352.68$  (54) Å<sup>3</sup>,  $Z = 4$ . These data are consistent with the published parameters of  $\alpha$ -BaCl<sub>2</sub> with the space group  $Pnma$  (#62) (Tab. 2, Fig. 4). Because of the geometric relationships of some of the unit cells of BaCl<sub>2</sub> polymorphs, we invested much effort into differentiation among the high-temperature cubic, metastable hexagonal, and monoclinic high-pressure BaCl<sub>2</sub> phases. Careful structural analysis showed that the natural phase described here clearly belongs to the orthorhombic polymorph.

According to Brackett et al. (1963) the  $\alpha$ -form of BaCl<sub>2</sub> exhibits a PbCl<sub>2</sub>-type (cotunnite) structure. There is a spread of Ba–Cl interatomic distances ranging 2.87–3.57 Å. Ba<sup>2+</sup> is coordinated by 9 Cl<sup>−</sup> ions on two inequivalent Cl<sup>−</sup> sites. In the first Cl<sup>−</sup> site, Cl<sup>−</sup> is tetrahedrally coordinated by four symmetrically equivalent Ba<sup>2+</sup> ions. In the second Cl<sup>−</sup> site, Cl<sup>−</sup> is bonded to five symmetrically equivalent Ba<sup>2+</sup> ions.

In this study, X-ray powder diffraction data could not be collected owing to the small amount of material available and its sensitivity to air. Roughly refined values from measured electron diffraction are in general

**Tab. 3** Measured X-ray diffraction data for vegrandisite, obtained from electron diffraction of 3 zone axes ([111], [122], [312]) and compared with the published calculated X-ray diffraction data (Liu and Eick 1989; Brackett et al. 1963).

$d$ meas [Å]	$d$ calc [Å] L&E 1989	$d$ calc [Å] B et al. 1963	$hkl$
6.08	6.05	6.04	101
n.obs.	4.72	4.71	002
4.20	4.23	4.23	011
4.06	4.06	4.06	110 E
n.obs.	4.05	4.04	102
n.obs.	3.94	3.93	200
3.76	3.73	3.72	111
3.61	3.64	3.63	201
3.09	3.08	3.07	112
3.00	3.03	3.02	210

n.obs. = not observable due to grain orientation and tilt limitations, E = extinct reflection observable due to double diffraction

**Tab. 2** Published unit-cell parameters ( $a$ ,  $b$ ,  $c$  in Å) of  $\alpha$ -BaCl<sub>2</sub> compared to those from this work.

Reference	Method	$a$	$b$	$c$
This work	SAED	7.80	4.71	9.60
Sahl (1963)	XRD-powder	7.878	4.731	9.415
Brackett et al. (1963)	XRD-powder	7.865	4.731	9.421
Haase and Brauer (1978)	XRD-powder	7.879	4.734	9.444
Liu and Eick (1989)	XRD-powder	7.881	4.7298	9.419
Shoulders and Gaume (2017)	XRD-powder	7.8776	4.7360	9.4357
Hull et al. (2011)	NPD-powder	7.8813	4.7369	9.4360
Ting et al. (2012)	NPD-powder	7.9693	4.7931	9.4922
Bohley et al. (2011)	Calculated (DFT)	7.72	4.66	9.26
Kumar and Vedeshwar (2015)	Calculated (DFT)	7.943	4.778	9.514

agreement with the published X-ray diffraction data (Tab. 3), but the precision is lower. This is due to the limited number of reflections, the limited tilt of the TEM holder and the small diffraction angles in electron diffraction (leading to only two significant digits for  $d$  values). Furthermore, the substitution of Sr for Ba and Br for Cl may affect the lattice parameters. However, there are many entries of powder XRD patterns of synthetic  $\alpha$ -BaCl<sub>2</sub> available in the JCPDS-ICDD (Joint Committee of Powder Diffraction Standards–International Centre for Diffraction Data; <https://www.icdd.com/>) database.

#### 4.4. Optical and spectroscopic properties

According to Wulff and Heigl (1931) and Winchel and Winchel (1989) synthetic orthorhombic BaCl<sub>2</sub> is biaxial (+), with refraction indices  $\alpha = 1.73024$  (15),  $\beta = 1.73611$  (15),  $\gamma = 1.74196$  (15), measured in sodium light with  $\lambda = 589$  nm. It is not pleochroic, angle  $2V$  is near 90° and molar refraction  $R$  is 21.36.

Polarized Raman measurements on synthetic orthorhombic BaCl<sub>2</sub> crystals were published by Sadoc and Guillo (1971) and Pfau et al. (2011). They spectra display strong vibration bands at around 113, 125, 152, 175 and 186 cm<sup>−1</sup>, accompanied by weaker but distinctive bands at about 55, 60, 76 and 200 cm<sup>−1</sup> (Tab. 4). Our own Raman measurements of synthetic BaCl<sub>2</sub> powder provided vibrational bands at 56, 77, **114**, **125**, 153, 176,

**Tab. 4** The Raman shift of main bands of synthetic  $\alpha$ -BaCl<sub>2</sub> (in cm<sup>−1</sup>) obtained in this study and compared to published experimental data by Pfau et al. (2011). The assignment of bands is based on calculations of Bohley et al. (2011).

$\alpha$ -BaCl <sub>2</sub>	$\alpha$ -BaCl <sub>2</sub> (Pfau et al. 2011)	Assignment of bands
56	55	A <sub>g</sub>
–	60	B <sub>1g</sub>
77	76	A <sub>g</sub>
<b>114</b>	<b>113</b>	B <sub>2g</sub>
<b>125</b>	<b>125</b>	B <sub>2g</sub> and B <sub>3g</sub>
153	152	B <sub>2g</sub>
176	175	A <sub>g</sub>
<b>187</b>	<b>186</b>	B <sub>3g</sub>
201	200	A <sub>g</sub>

187, 201 (strong bands in bold). In salt melt inclusions, recognition of the Raman spectrum of  $\alpha$ -BaCl<sub>2</sub> is difficult as this phase is very small and all major peaks of the spectrum overlap with the spectra of larger grains of other phases, having much stronger Raman signal (especially javorieite, hibbingite), and the host quartz (Fig. 5).

## 5. Discussion

### 5.1. Relation to other species, name justification

In the Nickel-Strunz classification, vegrandisite belongs to 3.DC class [oxyhalides, hydroxyhalides and related double halides with Pb (As, Sb, Bi), without Cu]. In

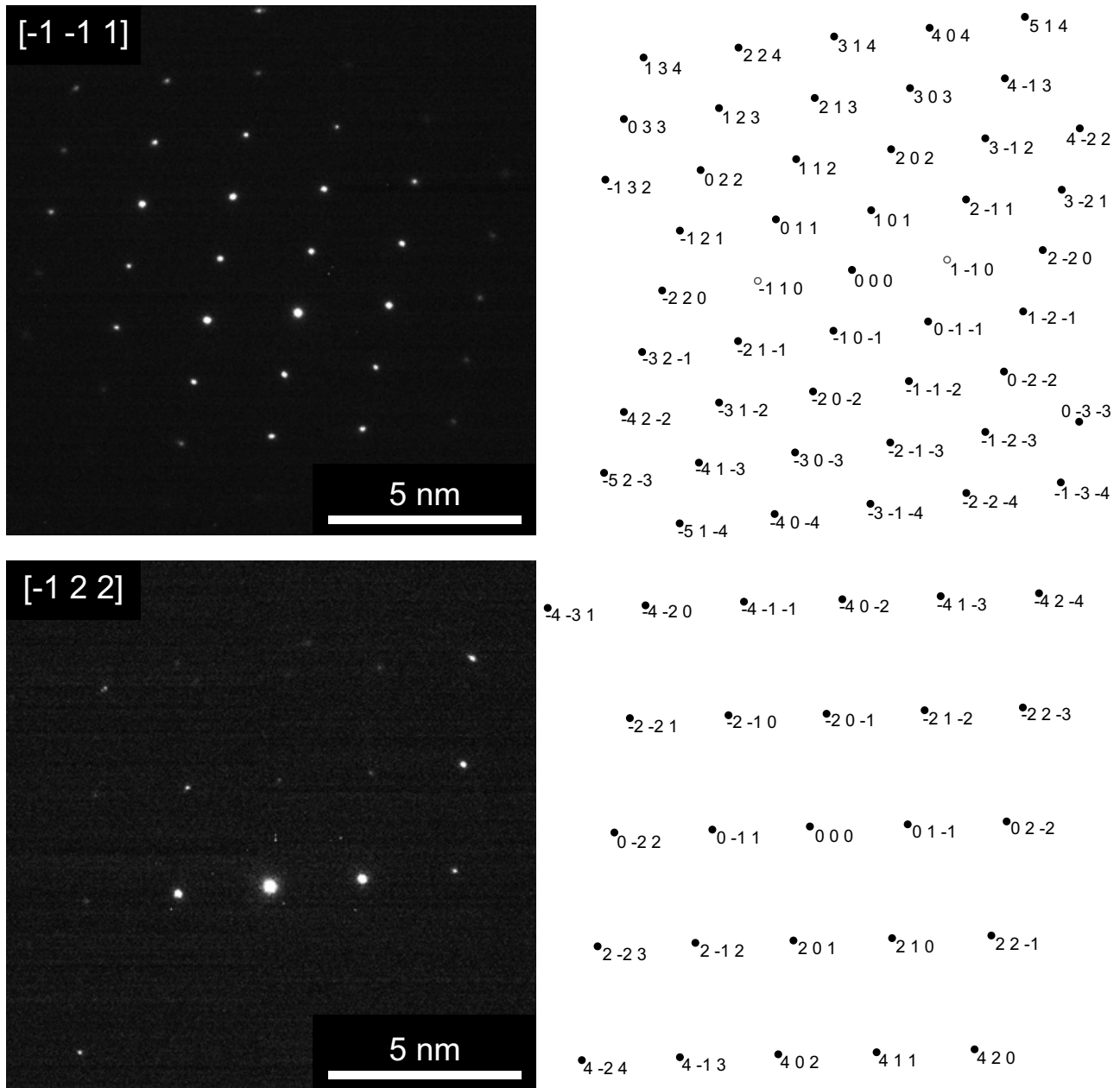


**Fig. 4** – Selected area diffraction patterns (SAED) taken from the area of the salt melt inclusion in quartz, from where TEM-EDX analyses provided composition close to that of vegrandisite from the sample DVE-51\_475.0 (left, see Fig. 2B). Images on the right show corresponding calculated simulations of diffraction patterns. Extra reflections in the SAED images, mostly visible in outer parts of the  $[\bar{1}\bar{2}2]$  zone axis, stem from the neighbouring crystal of hibbingite (due to the limited size of vegrandisite), and hot pixels of the CCD camera (due to the relative long acquisition time combined with the low diffraction intensity).

the Dana classification, it belongs to the 09.02.07 class cotunnite group (anhydrous and hydrated halides  $A(X)_2$ ).

The name of the mineral was derived from Latin *vegrandis* for small or tiny. It is the opposite of *grandis* – large.

## 5.2. Origin of the new mineral

The genesis of the mineral is closely linked to the specific origin of the parental salt melt at the porphyry gold deposit Biely Vrch (Koděra et al. 2014, 2018). The nearly water-free salt melt evolved from a hypersaline liquid, accompanied by magmatic vapor, that were exsolved from a dioritic magma emplaced at shallow subvolcanic depth (<3.5 km, ~850 °C). Increasingly Fe–K-rich salt melt evolved due to water loss to the vapor and halite precipitation during fluid cooling on ascent to the level of the porphyry intrusion (0.5–1 km). The salt melt was entrapped in the form of fluid inclusions in vein quartz and several solid phases have subsequently crystallized from the salt melt on cooling of the inclusions, including vegrandisite. Based on LA-ICP-MS microanalytical data, the major components of the inclusions are 50 wt. %  $FeCl_2$ , 30 wt. %  $KCl$  and 20 wt. %  $NaCl$  (Koděra et al. 2014). As the barium chloride crystals in salt melt inclusions always occur close to the contraction cavity in inclusions (Fig. 2), they probably belong to the last crystallizing solid phases. Thus, their crystallization temperature is probably not much higher than the temperature of first melting of salt melt inclusions (321–333 °C; Koděra et al. 2014), corresponding to the eutectic crystallization of the system  $NaCl$ – $KCl$ – $FeCl_2$  (Robelin et al. 2004). This is much lower than the melting point of  $BaCl_2$  (962 °C), however, alkali chlorides can significantly lower eutectics of molten salt system with barium chloride. A phase diagram of the system  $NaCl$ – $KCl$ – $FeCl_2$ – $BaCl_2$  is not available, but in the system  $NaCl$ – $KCl$ – $BaCl_2$ , the eutectic temperature is 543 °C (Takizawa et al. 2022), and in the system  $NaCl$ – $MgCl$ – $BaCl_2$ , it is just 422 °C (FactSage FTsalt molten salt database; [http://www.factsage.cn/fact/documentation/ftsalt/ftsalt\\_list.htm](http://www.factsage.cn/fact/documentation/ftsalt/ftsalt_list.htm)). The late

crystallization of  $BaCl_2$  is probably related to the increase in Ba content in the residual salt melt, as barium behaves as an incompatible element and the average barium content in inclusions is just about 5000 ppm. Note that due to the hydration properties of  $BaCl_2$  (Ropp 2013), this mineral can hardly crystallize from a hydrothermal fluid or evaporite brine. This explains the rare occurrence of this compound as a mineral in nature, as it can probably crystallize just from cooling anhydrous salt melts.

Another possible natural occurrence of a  $BaCl_2$  mineral was described from the Lindsley Cu–Ni–PGE mine of the Sudbury Igneous Complex in Canada. Farrow et al. (1994) determined here  $BaCl_2$  as a daughter mineral in several opened brine inclusions in quartz and chalcopyrite by quantitative SEM-EDS analyses. In the Lindsley mine, the  $BaCl_2$  phase is accompanied by halite, cotunnite ( $PbCl_2$ ), hibbingite and some other unknown K–Ca–Na and Fe–Mn chlorides (Farrow et al. 1994).

## 6. Conclusions

Minerals that are highly liable to hydration are often very difficult to identify, especially if they are of small size. In this work, we present the discovery of a mineral that has been known in inorganic chemistry for a long time,

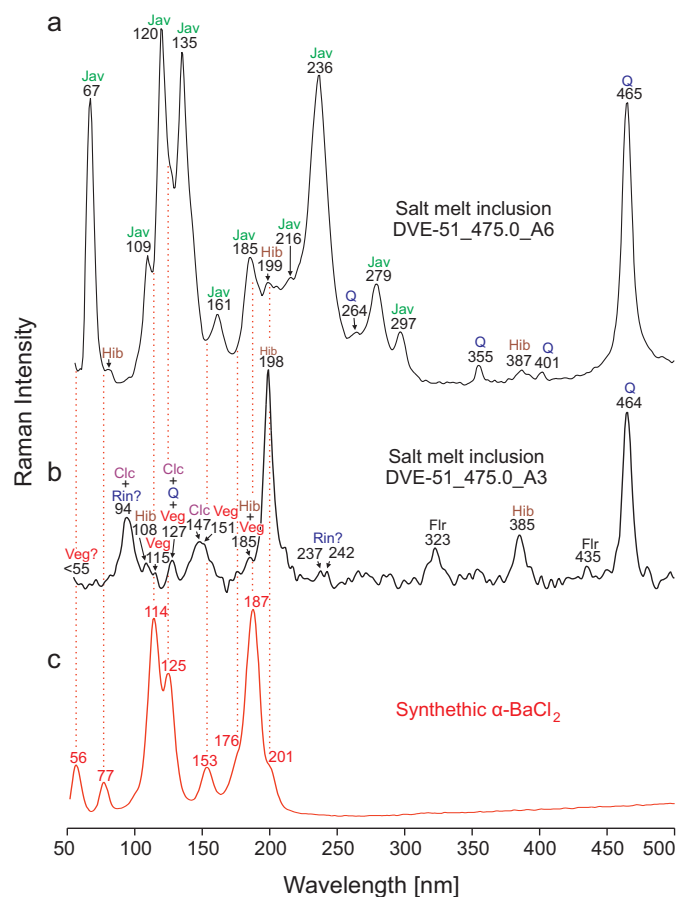


**Fig. 5** – Raman spectrum of synthetic  $\alpha$ - $BaCl_2$  compared to Raman spectra obtained from natural salt melt inclusion hosted in quartz from the Biely Vrch deposit. Assignment of Raman bands to solid phases is based on the published spectra of javorieite (Koděra et al. 2017), hibbingite (Koděra et al. 2022), chlorocalcite (Grishina et al. 2018), and rinneite (Grishina et al. 2020). **a** – Spectrum obtained from the point close to the studied vegrandisite in the inclusion in the sample DVE-51\_475.0. Strong signal from javorieite and hibbingite overprint the possible signal from vegrandisite. **b** – Spectrum from another inclusion from the same sample, where the Raman spectrum of vegrandisite can be distinguished from spectra of other phases in the inclusion (hibbingite, chlorocalcite, rinneite?, fluorite). **c** – Raman spectrum of synthetic  $\alpha$ - $BaCl_2$  (powder, this study). Veg = vegrandisite, Hib = hibbingite, Hl = halite, Jav = javorieite, Rin = rinneite, Flr = fluorite.

but it has never been determined in geological samples. Identification of the new mineral vegrandisite in the present study has been made possible through structural data of the mineral obtained from the FIB-TEM analytical technique. This technique enabled measurements of diffraction patterns of the same phase that was previously analysed by EDS. Using a combination of the two independent analytical tools, we have demonstrated an excellent match with  $\alpha$ -BaCl<sub>2</sub> at the chemical, atomic, and molecular levels, including unit-cell determination, which data have already been published for this chemical compound earlier.

Minerals in salt melt inclusions provide an insight into the unusual world of anhydrous salt minerals that can crystallize on cooling in this type of fluid inclusions. Vegrandisite (BaCl<sub>2</sub>) is a new mineral that occurs solely as a daughter mineral in nearly anhydrous salt melt inclusions at the Biely Vrch porphyry gold deposit in Slovakia. This is the second new mineral that was already identified in salt melt inclusions from this deposit (javorieite was the first one). Apparently, this specific hydrothermal system was operating as a natural chemical laboratory, enabling the growth of unique minerals that were previously known only in inorganic chemistry and materials science. Crystallisation of these phases occurred from nearly anhydrous, hot salt melts, trapped and cooled in the closed environment of inclusions in quartz, where they were protected from hydration and decomposition. Due to the subsequent increase in incompatible elements in residual salt melts on cooling, the occurrence and future discovery of other minor mineral phases is likely, although even with the combined application of unconventional methods this task will become more challenging due to the very small size of the phases and their high sensitivity to hydration and oxidation.

The identification of tiny minerals in crystallised salt melt inclusion helps to understand the behaviour of major and minor elements in cooling high salinity magmatic-hydrothermal systems. However, it also has a potential to contribute to chemical sciences in understanding of phase relations in complex chloride salt melts. On the other hand, some of the expected chloride minerals can be already well known in analytical chemistry, as was the case of vegrandisite in this contribution and javorieite in the past (Koděra et al. 2017), which helped to describe properties of the new minerals.

*Acknowledgements.* We appreciate constructive criticism and helpful comments by Roman Skála and David Vanko and the editorial handling by Jiří Zachariáš. This work was supported by the grants VEGA-1/0313/20 and APVV-22-0134.

## References

- BOHLEY C, WAGNER J-M, PFAU C, MICLEA P-T, SCHWEIZER S (2011) Raman spectra of barium halides in orthorhombic and hexagonal symmetry: An ab initio study. *Phys Rev B* 83: 024107
- BOSI F, HATERT F, PASERO M, MILLS SJ (2024) IMA Commission on New Minerals, Nomenclature and Classification (CNMNC) – Newsletter 80. *Eur J Mineral* 36: 599–604
- BRACKETT EB, BRACKETT TE, SASS RL (1963) The crystal structures of barium chloride, barium bromide and barium iodide. *J Phys Chemistry* 67: 2132–2135
- CAMPOS E, TOURET JLR, NIKOGOSIAN I, DELGADO J (2002) Overheated, Cu-bearing magmas in the Zaldívar porphyry-Cu deposit, Northern Chile. *Geodynamic consequences. Tectonophysics* 345: 229–251
- FARROW CEG, WATKINSON D, JONES P (1994) Fluid inclusions in sulfides from North and South Range Cu–Ni–PGE deposits, Sudbury Structure, Ontario. *Econ Geol* 89: 647–655
- FULIGNATI P, KAMENETSKY VS, MARIANELLI P, SBRANA A, MERNAGH TP (2001) Melt inclusion record of immiscibility between silicate, hydrosaline, and carbonate melts: Applications to skarn genesis at Mount Vesuvius. *Geology* 29: 1043–1046
- GRISHINA S, KODĚRA P, URIART L, DUBESY J, ORESHONKOV A, GORYANOV S, ŠIMKO F, YAKOVLEV I, ROGINSKII EM (2018) Identification of anhydrous CaCl<sub>2</sub> and KCaCl<sub>3</sub> in natural inclusions by Raman spectroscopy. *Chem Geol* 493: 532–543
- GRISHINA S, KODĚRA P, GORYANOV S, ORESHONKOV A, SERYOTKIN Y, ŠIMKO F, POLOZOV AG (2020) Application of Raman spectroscopy for identification of rinneite (K<sub>3</sub>NaFeCl<sub>6</sub>) in inclusions in minerals. *J Raman Spectr* 51: 2505–2516
- HAASE A, BRAUER G (1978) Hydratstufen und Kristallstrukturen von Bariumchlorid. *Z Anorg Allgem Chem* 441: 181–195
- HANES R, BAKOS F, FUCHS P, ŽITŇAN P, KONEČNÝ V (2010) Exploration results of Au porphyry mineralizations in the Javorie stratovolcano. *Miner Slovaca* 42: 15–33
- HOLLAND JB, REDFERN S (1997) Unit cell refinement from powder diffraction data: the use of regression diagnostics. *Mineral Mag* 61: 65–77
- HULL S, NORBERG ST, AHMED I, ERIKSSON SG, MOHN CE (2011) High temperature crystal structures and superionic properties of SrCl<sub>2</sub>, SrBr<sub>2</sub>, BaCl<sub>2</sub> and BaBr<sub>2</sub>. *J Solid State Chem* 184: 2925–2935
- KIM MJ, KIM HJ, PARK H, KIM S, KIM J (2011) Characterization of BaCl<sub>2</sub> scintillation crystal at low temperature. *Nucl Instrum Methods Phys Res A* 632: 47–51
- KODĚRA P, HEINRICH CA, WÄLLE M, LEXA J (2014) Magmatic salt melt and vapour: Extreme fluids forming porphyry gold deposits in shallow volcanic settings. *Geology* 42: 495–498

- KODĚRA P, TAKÁCS A, VÁCZI T, LUPTÁKOVÁ J, ANTAL P (2015) Mineral composition of salt melt inclusions of the porphyry gold deposit Biely Vrch (Slovakia). In: Ext Abstr Vol XXIII ECROFI Conf, pp 86–87
- KODĚRA P, TAKÁCS A, RACEK M, ŠIMKO F, LUPTÁKOVÁ J, VÁCZI T, ANTAL P (2017) Javorieite,  $KFeCl_3$ : a new mineral hosted by salt melt inclusions in porphyry gold systems. *Eur J Miner* 29: 995–1004
- KODĚRA P, KOZÁK J, BRČEKOVÁ J, CHOVAN M, LEXA J, JÁNOŠÍK M, BIROŇA, UHLÍK P, BAKOS F (2018) Distribution and composition of gold in porphyry gold systems: example from the Biely Vrch deposit, Slovakia. *Miner Depos* 53: 1193–1212
- KODĚRA P, MAJZLAN J, POLLOK K, KIEFER S, ŠIMKO F, SCHOLTZOVÁ E, LUPTÁKOVÁ J, CAWTHORN G (2022) Ferrous hydroxychlorides hibbingite ( $\gamma\text{-Fe}_2(\text{OH})_3\text{Cl}$ ) and parahibbingite ( $\beta\text{-Fe}_2(\text{OH})_3\text{Cl}$ ) as a concealed sink of Cl and  $\text{H}_2\text{O}$  in ultrabasic and granitic systems. *Am Mineral* 107: 826–841
- KOZÁK J, KODĚRA P, LEXA J, BAKOS F, MOLNÁR L, WÄLLE M (2017) Porphyry gold system of Beluj in the mantle of the Štiavnica stratovolcano (Slovakia). *Acta Geol Slovaca* 9: 45–61
- KUMAR P, VEDESHWAR AG (2015) DFT calculations of structural, electronic, optical and elastic properties of scintillator materials  $\text{BaCl}_2$  and  $\text{BaBr}_2$ . *J Phys D: Appl Phys* 48: 105301
- LEXA J, ŠTOHL J, KONEČNÝ V (1999) Banská Štiavnica ore district: relationship among metallogenetic processes and geological evolution of a stratovolcano. *Miner Depos* 34: 639–665
- LIDLE DR (ed.) (2010) CRC handbook of chemistry and physics (90th ed., Internet version). CRC Press/Taylor and Francis, Boca Raton, FL <https://doi.org/10.1002/jctb.280500215>
- LIU G, EICK, HA (1989) Solvolytic decomposition studies on mixed phases: Synthesis of the anti- $\text{Fe}_2\text{P}$ -type  $\text{BaX}_2$  ( $X \equiv \text{Cl}, \text{Br}$ ) from  $\text{BaX}_2$ ,  $\text{LnX}_3$  phases. *J Less-Common Metals* 149: 47–53
- PFAU C, BOHLEY C, MICLEA P-T, SCHWEIZER S (2011) Structural phase transitions of barium halide nanocrystals in fluorozirconate glasses studied by Raman spectroscopy. *J Appl Phys* 109: 083545
- RICHARDS TW (1894) Neubestimmung des Atomgewichts von Baryum. Zweite Abhandlung. Analyse von Baryumchlorid, *Z Anorg Chem*, 6, 89–127
- ROBELIN C, CHARTRAND P, PELTON AD (2004) Thermodynamic evaluation and optimization of the ( $\text{NaCl} + \text{KCl} + \text{MgCl}_2 + \text{CaCl}_2 + \text{MnCl}_2 + \text{FeCl}_2 + \text{CoCl}_2 + \text{NiCl}_2$ ) system. *J Chem Thermodyn* 36: 809–828
- ROPP, RC (2013) Encyclopedia of the Alkaline Earth Compounds. Elsevier
- ROTTIER B, KOUZMANOV K, BOUVIER AS, BAUMGARTNER LP, WÄLLE M, REZEAU H, BENDEZÚ R, FONTBOTÉ L (2016) Heterogeneous melt and hypersaline liquid inclusions in shallow porphyry type mineralization as markers of the magmatic-hydrothermal transition (Cerro De Pasco district, Peru). *Chem Geol* 447: 93–116
- SADOC A, GUILLO R (1971) Spectres Raman de  $\text{SrCl}_2$ ,  $\text{BaCl}_2$  et  $\text{PbCl}_2$ . *C R l'Acad Sci Sér B* 273: 203–207
- SAHL K (1963) Die Verfeinerung der Kristallstrukturen von  $\text{PbCl}_2$  (Cotunnit),  $\text{BaCl}_2$ ,  $\text{PbSO}_4$  (Anglesit) und  $\text{BaSO}_4$  (Baryt). *Beitr Miner Petrogr* 9: 111–132
- SHOULDERS WT, GAUME RM (2017) Phase-change sintering of  $\text{BaCl}_2$  transparent ceramics, *J Alloys Comp* 705: 517–523
- SIMÓN V, KODĚRA P, LÜDERS V, TRUMBULL RB, ARNOSIO M, BUSTOS E, DESANOIS L, SOŚNICKA M, WOHLGEMUTH-UEBERWASSER C (2024) Fluid evolution of the Lindero porphyry gold deposit, NW Argentina: the critical role of salt melts in ore formation. *Miner Depos* 59: 1455–1477
- TAKIZAWA Y, KAMADA K, KIM KJ, YOSHINO M, YAMAJI A, KUROSAWA S, YOKOTA Y, SATO H, TOYODA S, OHASHI Y, HANADA T, KOCHURIKHIN VV, YOSHIKAWA A (2022) Large size growth of terbium doped  $\text{BaCl}_2/\text{NaCl}/\text{KCl}$  eutectic for radiation imaging. *Japan J Appl Phys* 61: SC1009
- TING VP, HENRY, PF, SCHMIDTMANN M, WILSON CC, WELLER MT (2012) Probing hydrogen positions in hydrous compounds: information from parametric neutron powder diffraction studies. *Phys Chemistry Chem Phys* 14: 6914–6921
- WINCHELL AN, WINCHELL H (1989) The microscopic characters of artificial inorganic solid substances or artificial minerals, 3rd edition. McCrone Res Inst, Chicago, IL, pp 1–410
- WULFF P, HEIGL A (1931) Refraktometrische Messungen an Kristallen. *Z Kristallogr* 77: 84–121
- XU X, XU X, SZMIHESKY M, YAN J, XIE Q, STEELE-MACINNIS M (2023) Melt inclusion evidence for limestone assimilation, calc-silicate melts, and magmatic skarn. *Geology* 51: 491–495
- XU XY, BAIN WM, TORNOS F, HANCHAR JM, LAMADRID HM, LEHMANN B, XU XC, STEADMAN JA, BOTTRILL RS, SOLEYMANI M, RAJABI A, LI P, TAN X, XU S, LOCOCK AJ, STEELE-MACINNIS M (2024) Magnetite-apatite ores record widespread involvement of molten salts. *Geology* 52: 417–422